Ocean Dynamics
DOI 10.1007/s10236-014-0788-4

The wind sea and swell waves climate in the Nordic seas

Alvaro Semedo · Roberto Vettor · Øyvind Breivik · Andreas Sterl · Magnar Reistad · Carlos Guedes Soares · Daniela Lima

Received: 5 March 2014 / Accepted: 20 October 2014

Abstract A detailed climatology of wind sea and swell waves in the Nordic Seas (North Sea, Norwegian Sea, and Barents Sea), based on the high-resolution reanalysis NORA10, developed by the Norwegian Meteorological Institute, is presented. The higher resolution of the wind forcing fields, and the wave model (10 km in both cases), along with the inclusion of the bottom effect, allowed a better description of the wind sea and swell features, compared to previous global studies. The spatial patterns of the swell-dominated regional wave fields are shown to be different from the open ocean, due to coastal geometry, fetch dimensions, and island sheltering. Nevertheless, swell waves are still more prevalent and carry more energy in the Nordic Seas, with the exception of the North Sea. The influence of the North Atlantic Oscillation on the winter regional wind sea and swell patterns is also presented. The analysis of the decadal trends of wind sea and swell heights during the NORA10 period (1958–2001) shows that the long-term trends of the total significant wave height (SWH) in the Nordic Seas are mostly due to swell and to the wave propagation effect.

Keywords Wind sea · Swell · Wave climate · Air-sea interaction · Wave age · NORA10 · Nordic Seas · North Atlantic Oscillation

Responsible Editor: Alexander V. Babanin

This article is part of the Topical Collection on the *13th International Workshop on Wave Hindcasting and Forecasting in Banff, Alberta, Canada October 27–November 1, 2013*

A. Semedo (✉) · D. Lima
Escola Naval-CINAV, Base Naval de Lisboa, Alfeite, Almada 2810-001, Portugal
e-mail: milho.semedo@marinha.pt

A. Semedo
Department of Earth Sciences, Uppsala University, Uppsala, Sweden

A. Semedo · R. Vettor · C. G. Soares
Centre for Marine Technology and Engineering (CENTEC), Instituto Superior Técnico, Universidade de Lisboa, Lisbon, Portugal

Ø. Breivik
European Centre for Medium-Range Weather Forecasts, Reading, UK

A. Sterl
Royal Netherlands Meteorological Institute (KNMI), De Bilt, Netherlands

M. Reistad
Norwegian Meteorological Institute, Oslo, Norway

A. Semedo · D. Lima
Instituto Dom Luiz, University of Lisbon, Lisbon, Portugal

1 Introduction

Ocean surface gravity waves, also called wind waves, are the most obvious air-sea interaction phenomena at the interface between the atmosphere and the ocean. Wind waves (henceforth, simply called waves) account for most of the energy carried by all waves at the ocean surface (Kinsman 1965). Waves also have a significant impact on offshore and coastal infrastructures, ship design and routing, beach erosion and sediment transport, for example, and are an important element in extreme events, like storm surges and flooding in coastal areas. There are two types of waves at the ocean surface: wind sea and swell. Wind sea waves (also called young or growing waves) are waves under the influence of local winds. As waves propagate away from their generation area, or when their phase speed overcomes the local wind speed, they are called swell. Swell waves can propagate thousands of kilometers across entire ocean basins (Snodgrass et al. 1966; Alves 2006), with energy *e*-folding scales exceeding 20,000 km (Ardhuin et al. 2009).

Published online: 08 November 2014

The most common parameters used to characterize sea states are the significant wave height (SWH) and the mean wave period (MWP). But these two parameters provide a limited description of the wave field. They are calculated by integrating the wave spectra, and two wave fields with the same SWH and MWP may still be very different in detail, in the sense that they can be more or less dominated by one type of waves; a mixed sea state of wind sea and swell waves can have the same SWH and MWP as a younger sea state with a very strong prevalence of wind sea waves almost without swell (Holthuijsen 2007; Semedo et al. 2011a). For this reason, a more detailed investigation and qualitative analysis is needed to correctly define the wave field characteristics and climate of a certain area. The way to pursue this analysis is by studying the wind sea and swell parameters separately (Guedes Soares 1984): SWH and MWP, but also mean wave direction (MWD).

The qualitative analysis of ocean surface waves has been the focus of several recent global studies, from the wave climate community (Chen et al. 2002; Gulev and Grigorieva 2006; Semedo et al. 2011a; Fan et al. 2014), but also from the air-sea interaction community (Smedman et al. 2009; Högström et al. 2009, 2013; Hanley et al. 2010; Semedo et al. 2009; Nilsson et al. 2012; Rutgersson et al. 2012; Belcher et al. 2012). The reason for this interest lies mostly in the fact that waves have an impact on the lower atmosphere, and that the air-sea coupling is different depending on the wave regime, be it wind sea or swell dominated (Cavaleri et al. 2012). Waves modulate the exchange of momentum, heat, and mass across the air-sea interface (Janssen 2012; Janssen et al. 2013), and this modulation is different and dependent on the prevalence of one type of waves: wind sea or swell (Högström et al. 2009; Semedo et al. 2009). During the wave growth process, the momentum flux is directed downward, and the wave impact on the atmosphere is restricted to a very shallow layer, of the order of 1 m. When the ocean surface is dominated by swell, particularly during light winds, waves dissipate energy to the atmosphere as they propagate (Ardhuin and Jenkins 2006). In this situation, the net momentum flux can reverse its direction, from downward to upward. It has been observed that in certain conditions, due to this momentum flux reversal, waves "accelerate" the wind in the first meters above the water, producing a jet-like feature, and introducing a departure from the logarithmic wind profile. These "wave driven" wind speed departures reduce the wind shear and, consequently, the mechanical production of turbulence (Smedman et al. 1999; Sullivan et al. 2008) and are responsible for the collapsing of the lower atmosphere turbulence structure (Högström et al. 2009).

The best way to produce reliable wave climate statistics would be to rely on buoy observations. However, and in spite of their accuracy, in situ wave measurements still have several problems, since they are found disproportionately near the coasts of industrialized countries, mostly in the northern hemisphere. The wave observations time series also suffer from inhomogeneities due to changes in instrument type and location (see Bidlot et al. 2002), and, most notably, their very sparse geographical distribution and data gaps do not allow their use for wave climate studies in large areas. Remote sensing wave measurements are an alternative, but the length of the time series, as well as the poor temporal resolution of the polar-orbiting satellites, are problems that still limit its use for accurate wave climate studies. On the other hand, spectral partitioning is the best way to isolate wind sea and swell characteristics (Gerling 1992; Hanson and Phillips 2001), and, up to the moment, long enough and sufficiently accurate spectral descriptions of the wave field are only available from wave model hindcasts and reanalyses.

Recently, several global long-term wave climate studies, using wave hindcasts or reanalyses, were published in the literature (Chawla et al. 2012; Stopa and Cheung 2014; Fan et al. 2012), but only one had a particular focus on wind sea and swell waves climate: Semedo et al. (2011a), whom, using ERA-40 reanalysis data (Uppala and Coauthors 2005; Sterl and Caires 2005), presented a detailed global climatology of both wave regimes (wind sea and swell). They have shown that the global ocean is dominated by swell waves: that they carry most of the energy at the ocean surface, and that the probability of having swell dominated wave fields is substantially higher than the probability of having wind sea dominated fields. This is true even for the mid to high latitudes, along the extratropical storm tracks, where the wind speed and the relative weight of the wind sea part of the wave spectra are highest. Chen et al. (2002), and later Jiang and Chen (2013), using shorter time series of blended remote sensing and wave model data, also reached similar conclusions regarding the swell prevalence in the open ocean.

Global reanalyses do not resolve mesoscale dynamics nor do they come close to modeling coastal wind and wave features. In regional areas, coastal and other mesoscale effects on the wind regimes compete with larger scale forcings, but also fetches are variable and depend on the wind direction. Bottom topography also adds additional complexity. For these reasons, the wind sea and swell regimes in coastal waters and in marginal seas are expected to be substantially different (and dynamic) when compared to open-ocean areas. Model resolution, therefore, is an important issue in modeling regional wind sea and swell features.

Some (few) long-term regional wave climate studies using downscaled wave hindcasts were recently pursued (e.g., Weisse and Günther 2007; Pilar et al. 2008; Lionello and Galati 2008; Lucas et al. 2011; Tuomi et al. 2011; Bosserelle et al. 2011), but none studied the wind sea and swell waves separately. In fact, to our knowledge, no regional wave climate study has looked at the qualitative analysis of wind sea and swell waves.

The goal of this study is to present a detailed climatology of wind sea and swell characteristics in the North Sea, Norwegian

Sea, Greenland Sea, and Barents Sea (henceforth called for convenience "the Nordic Seas"), based on the high-resolution Norwegian reanalysis at 10 km (NORA10, Reistad et al. 2011). The NORA 10 is a regional dynamical downscaling of the ERA-40 reanalysis (Uppala and Coauthors 2005), comprising both atmospheric and wave parameters, where considerable improvements in the mean and upper percentiles of wind speed and SWH were achieved, as well as improvements in the MWP (Reistad et al. 2011). The regional distribution of the wind sea and swell SWH and MWD parameters from NORA10, and how they combine in the total SWH and MWP, are presented. The long-term trends of SWH and its wind sea and swell components in these semi-enclosed seas are also analyzed.

The paper is outlined as follows. The NORA10 reanalysis is described in section 2. Section 3 presents the climatology of the regional wind sea and swell characteristics. The long-term variability of wind sea and swell heights in the Nordic Seas and how they combine in the overall SWH variability are presented in section 4. The paper ends with concluding remarks and suggestions for further research in section 5.

2 Data and analysis methodology

2.1 NORA10

A reanalysis is a rerun of the past, with the goal of overcoming inhomogeneities due to model and data assimilation changes, using as many observations available as possible. The best available model and data assimilation schemes, now kept unchanged in time during the integration, are used to repeat the analysis procedure. Inhomogeneities still prevail, unfortunately, due to uneven data coverage and changes in observation systems (Uppala 1997; Sterl 2004). We distinguish between reanalyses, which incorporate data assimilation, and wave hindcasts, which are model-only exercises without data assimilation. NORA10 is a high-resolution regional downscaling of the ERA-40 reanalysis (Uppala and Coauthors 2005) produced by the Norwegian Meteorological Institute (Reistad et al. 2011). It is a hybrid between a reanalysis and a hindcast in the sense that the wave model (WAM) has no data assimilation and thus relies solely on the wind forcing and the boundary conditions, while the atmospheric model has been initialized from the ERA-40 reanalysis and as such is a downscaled reanalysis (but with no additional data assimilation).

In NORA10, no coupled model system is used, as was in ERA-40 (Bidlot 2001), and the atmospheric and wave downscalings were done separately. First, the atmospheric reanalysis was produced with the hydrostatic High-Resolution Limited-Area Model (HIRLAM; Undén and Coauthors 2002) at 10–11-km resolution (HIRLAM10), with 40 vertical levels, more densely spaced near the surface. The model domain was set up as a rotated spherical grid (Reistad et al. 2011). The HIRLAM model was forced at the boundaries with temperature, wind, specific humidity, and cloud water, at all vertical levels, plus surface pressure, with a 6-hourly temporal resolution. Sea surface temperature was interpolated from ERA-40. The wave hindcast was then produced by forcing the wave model WAM (cycle 4; WAMDI Group 1988; Komen et al. 1994) with HIRLAM10 winds on the same domain as the atmospheric model domain. The inner 10–11-km resolution wave model domain was nested in a larger 50-km resolution domain that generated boundary conditions (see Breivik et al. 2009 for details on the nesting). The outer domain was forced with ERA-40 winds. Ice coverage information was passed to the wave model from HIRLAM10 three times per month. Both outer and inner domains were integrated with the bottom friction mode on.

The results of NORA10 show a significant improvement of coastal and open-ocean winds, and therefore, also a significant improvement of the downscaled wave fields. Further details and results on the performance of NORA10 are presented by Reistad et al. (2011), while Aarnes et al. (2012) and Breivik et al. (2013) analyze the tail behavior and the estimated return values derived from NORA10.

In NORA10, all atmospheric and wave parameters are archived on the native rotated latitude-longitude grid. The temporal resolution of the archive is 3 h. ERA-40 covers a period from September 1957 to August 2002. NORA10 has been extended beyond August 2002 using operation analyses from the ECMWF as boundary and initial conditions allowing for a longer data time series. Here, we use only the NORA10 period coincident with ERA-40, and from those, only the 1958–2001 period, allowing some degree of comparison with the results of Semedo et al. (2011a).

2.2 Wave parameters and spectral separation

The wave model WAM outputs two-dimensional wave energy spectra $F(f,\theta)$ at each grid point by integrating the so called wave energy balance equation (Holthuijsen 2007), where f and θ are the wave frequency and propagating direction, respectively. From the $F(f,\theta)$ spectra, several integrated wave parameters can be obtained. In the present study, the SWH and MWD from the total $(H_s,\ \theta_m)$, wind sea $\left(H_s^w,\ \theta_m^w\right)$, and swell $\left(H_s^s,\ \theta_m^s\right)$ wave fields, respectively, are used. Besides, the wave fields the NORA10 10-m wind speed (U_{10}) and direction (φ) are also used here. The SWH (Munk 1944) is defined as $SWH = H_s = 4.04\sqrt{m_0}$, where m_0 is the zeroth spectral moment, defined as

$$m_0 = \iint f^0 F(f,\theta) df d\theta, \tag{1}$$

and the MWD is defined as θ_m=atan(SF/CF), where

$$SF = \iint \sin(\theta) F(f,\theta) df d\theta \ \text{ and} \tag{2a}$$

$$CF = \iint \cos(\theta) F(f,\theta) df d\theta \tag{2b}$$

In the wave model WAM, the wind sea and swell parameters are obtained by integrating the high and low frequency parts of the wave spectra, respectively. The spectral partitioning is obtained through a separation frequency $\widehat{f}$, with a corresponding wave phase speed defined as

$$\widehat{c} = 33.6 \times u_* \cos(\theta - \varphi), \tag{3}$$

where u_* is the friction velocity. See Bidlot (2001) and Semedo et al. (2011a) for further details on the WAM wind sea and swell separation scheme.

The NORA10 wind and wave parameters were processed for seasonal means, following the World Meteorological Society seasonal partition: December-January-February (DJF), March-April-May (MAM), June-July-August (JJA), and September-October-November (SON). Here, we look only at the extreme seasons DJF and JJA (boreal winter and summer, respectively), in spite of some remarks in the text concerning the intermediate seasons MAM and SON.

3 The Nordic Seas wind sea and swell climates

3.1 Regional wind sea and swell-significant wave heights

The seasonal maps of the DJF and JJA U_{10} and φ (arrows) climatological means are shown in Fig. 1. The wind direction arrows are not scaled with the wind speed background field. The mean φ (as the total, wind sea, and swell mean wave directions θ_m, θ_m^w, and θ_m^s, respectively) was computed by averaging its zonal and meridional components separately.

The climatological amplitude of the near surface wind speed in the Nordic Seas between DJF and JJA, which is characteristical of the North Atlantic sub-basin (see Sterl and Caires 2005 and Semedo et al. 2011a), is noticeable in Fig. 1, although less pronounced than in the open ocean. During winter, the U_{10} is higher than 11 ms^{-1} in almost all the Nordic Seas, including in the North Sea, and higher than 12 ms^{-1} south of Iceland. In the summer, the climatological mean U_{10} is lower (less than 7 ms^{-1} in most of the area of interest), with a maximum (around 9 ms^{-1}) also south of Iceland. The Norwegian Sea is the preferred track of the extratropical storms in the North Atlantic (Chang et al. 2002; Bengtsson et al. 2006), and that can be seen in the southern areas of the domain, between Iceland and Scotland, where wind speeds are highest. In the South of Iceland, the surface winds are predominantly south-westerly, as part of the North Atlantic Westerlies, turning slightly counterclockwise as they enter the Norwegian Sea, both in DJF and JJA. This backing of the wind direction is part of the flow around of the Icelandic Low and is more noticeable in JJA. North of about 68° N, also in both seasons, the winds blow from the northeast, as part of the northern hemisphere Polar Easterlies. The convergence of the Westerlies with the Polar Easterlies (at the surface), marking the climatological Polar Front in this area, can be seen in both seasons, taking place slightly more North in JJA. Mesoscale features (not noticeable in ERA-40 winds; Sterl and Caires 2005; Semedo et al. 2011a) can be identified in the Barents Sea in both seasons, and along the western coast of Norway in JJA (most probably sea breezes). A slight increase in U_{10} in the Nordic Seas in DJF and JJA is noticeable when compared to ERA-40 (see Semedo et al. 2011a), confirming the results of Reistad et al. (2011), where the improvement of the surface wind speeds quality in NORA10 is shown.

Figure 2 displays the seasonal maps of H_s, H_s^s, and H_s^w (as well as of θ_m, θ_m^w, and θ_m^s, represented as arrows) climatological means for DJF and JJA. The most striking feature is the comparison of the magnitudes of H_s^s and H_s^w fields, in both seasons. While in the open ocean, H_s^s is considerably higher than H_s^w, as shown by Semedo et al. (2011a); this is not necessarily the case in smaller and constrained areas like the Nordic Seas, where the fetches are limited and swell waves do not have enough space to propagate away from their generation area. In DJF, the mean H_s^s and H_s^w are comparable, with the swell waves propagating into the Norwegian Sea, away from the H_s climatological maximum located south of Iceland. In both seasons, in the south of Iceland, H_s^s is slightly higher than H_s^w (around 3 m and 2.5 m in DJF, and around 1.5 m and 1 m in JJA, for H_s^s, and H_s^w, respectively). That does not happen in the North Sea, where wind sea waves are higher than swell waves in DJF (around 2 m and less than 1 m, respectively), and about the same height in JJA (around 0.8 m). In that marginal sea, due to its shape, but also to the sheltering effect of Great Britain, the H_s^s climatological means are almost the same in DJF and JJA, regardless of the seasonal wave heights amplitude differences in the open ocean and in the Norwegian Sea. In the northern part of the Norwegian Sea and in the Barents Sea, the mean H_s^s is also practically the same in winter and summer. That is not the case for H_s^w. Swells are slightly higher than wind seas in DJF in the northern part of the Norwegian Sea (around 2.5 m and 2.1 m, respectively), but lower in most parts of the Barents Sea due to the orientation of the fetch and to the sheltering effect of the Scandinavian Peninsula. The swell and wind sea mean directions are also very different in that area in both seasons, with the θ_m^w clearly reflecting westerlies and polar easterlies, while θ_m^s follows the propagation pattern into the Norwegian Sea from southwest. In JJA, the H_s^s climatological mean is higher than the H_s^w one in that area (north Norwegian Sea and Barents Sea), reflecting the low wind speeds at the surface

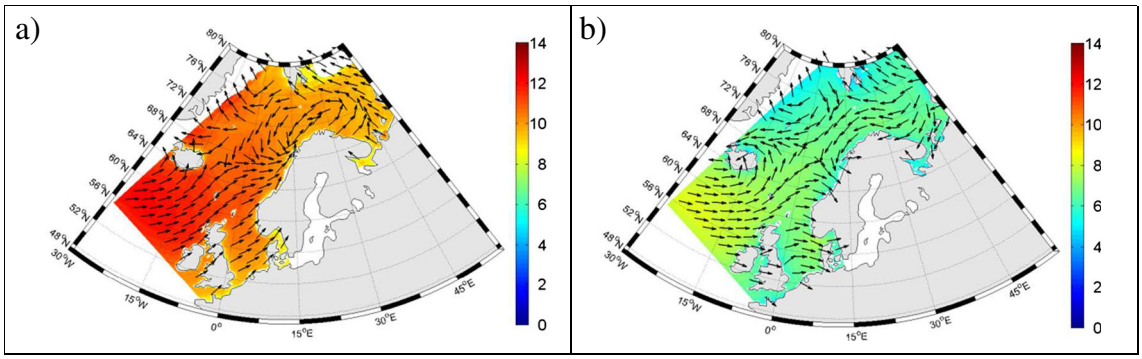

Fig. 1 Seasonal averages of $U_{10}(m\ s^{-1})$ and φ (°) for **a** DJF and **b** JJA. The *arrows* are not scaled with the background fields

shown in Fig. 1. As can be seen, the sheltering effect and the orientation of the fetch, compared to the coast lines and to the wind direction, are of great importance in the definition of the swell and wind sea wave climates in the Nordic Seas. This situation is different in the open ocean, where fetches are most of the times "infinite", waves can propagate freely, and the mean H_s^s is most of the times higher than the mean H_s^w (Semedo et al. 2011a; Jiang and Chen 2013; Fan et al. 2014).

Maps of the DJF mean H_s, H_s^s, and H_s^w 99 % percentiles (computed separately for each season and then averaged) are shown in Fig. 3. The 99 % percentiles for JJA are not shown because the extremes analysis was not relevant. Although the winter Nordic Seas wave field can be said, to a good degree, to be dominated by swell waves (since, as seen in Fig. 2, $H_s^s > H_s^w$ in most areas), that is clearly not the case for the extreme wave heights, where the total wave field is dominated by local wind sea waves. In an area south of Iceland, extending east towards the Faroe Islands, 1 % of the waves have a significant wave height of 11 m or higher. In almost the whole Norwegian Sea, that value is slightly lower, but close to 10 m. While the DJF mean 99 % percentile of H_s^w is comparable to the H_s pattern, although slightly more constrained, particularly in the highest wave heights area south of Iceland, the extreme H_s^s values are lower (less than 6 m and lower than that in the northern part of the domain). For the reasons mentioned above, the 99 % percentiles of H_s^s and H_s^w in the sheltered North Sea are different from the "open" Norwegian Sea, since there, the relative differences between the extreme wind sea and swell wave heights are even higher.

3.2 Regional wind sea and swell dominances

The predominance of one type of waves to the other can also be accessed through the wave age parameter. The wave age parameter was developed along with the sheltering hypotheses of Jeffreys (1924, 1925) to designate the characteristic wave phase speed normalized by a measure of the wind speed at a certain height, which latter was convened to be at 10 m height, and express the relative speed between the peak wave and the wind at a certain height, (c_p/U_{10}, where c_p is the peak wave phase speed). From the wave age parameter, the development of the sea state is characterized as dominated by wind sea if $c_p/U_{10} < 1.2$, or as dominated by swell if $c_p/U_{10} > 1.2$, according to the Pierson and Moskowitz spectrum (Pierson and Moskowitz 1964; Smith et al. 1992; Alves et al. 2003).

The characterization of the wave field by the wave age parameter implies that most of the wave energy has to be contained around the peak wave in the wave spectrum, which might not always be the case, particularly under the influence of heavy storms, where the spectrum width can be large and the wave energy be spread through a wider frequency band. Also, given the complexity of the wave field, the classification of the sea state into either swell or wind sea dominated can be seen as simplistic. Nevertheless, the wave age parameter gives a statistically meaningful qualitative description of the sea surface (Semedo et al. 2011a, b). Also, the wave age parameter has been largely used in different aspects of the air-sea interaction theory (Csanady 2003), namely in practical modeling solutions of wave-atmosphere coupled model systems (e.g., Lionello et al. 1998; Janssen et al. 2002; Rutgerson et al. 2010, 2012), where the feedback of the waves to the winds is modeled via a wave age dependent Charnock parameter (Charnock 1955, 1958).

To avoid the smoothing of the peaks of the wave age, we do not look at its means, but follow instead a probabilistic (frequency of occurrence) approach in assessing the wave field characteristics in terms of the wave type prevalence. To quantify the frequency of occurrence of the swell-dominated wave fields in the Nordic Seas, the parameter $P_s = N_s/N$ is computed for each grid point, where N_s is the number of swell-dominated events (i.e., the number of times where $c_p/U_{10} > 1.2$), and N is the total number of events. Following the approach of Chen et al. (2002) and Semedo et al. (2011a), the probabilistic parameter can also be defined as $P_s = P\left[c_p/U_{10} > 1.2\right]$, i.e., the probability (P) of having a swell-dominated wave field. The probability of having a wind sea dominated wave field (not shown) can therefore be defined as $P_w = 1 - P_s = P\left[c_p/U_{10} < 1.2\right]$.

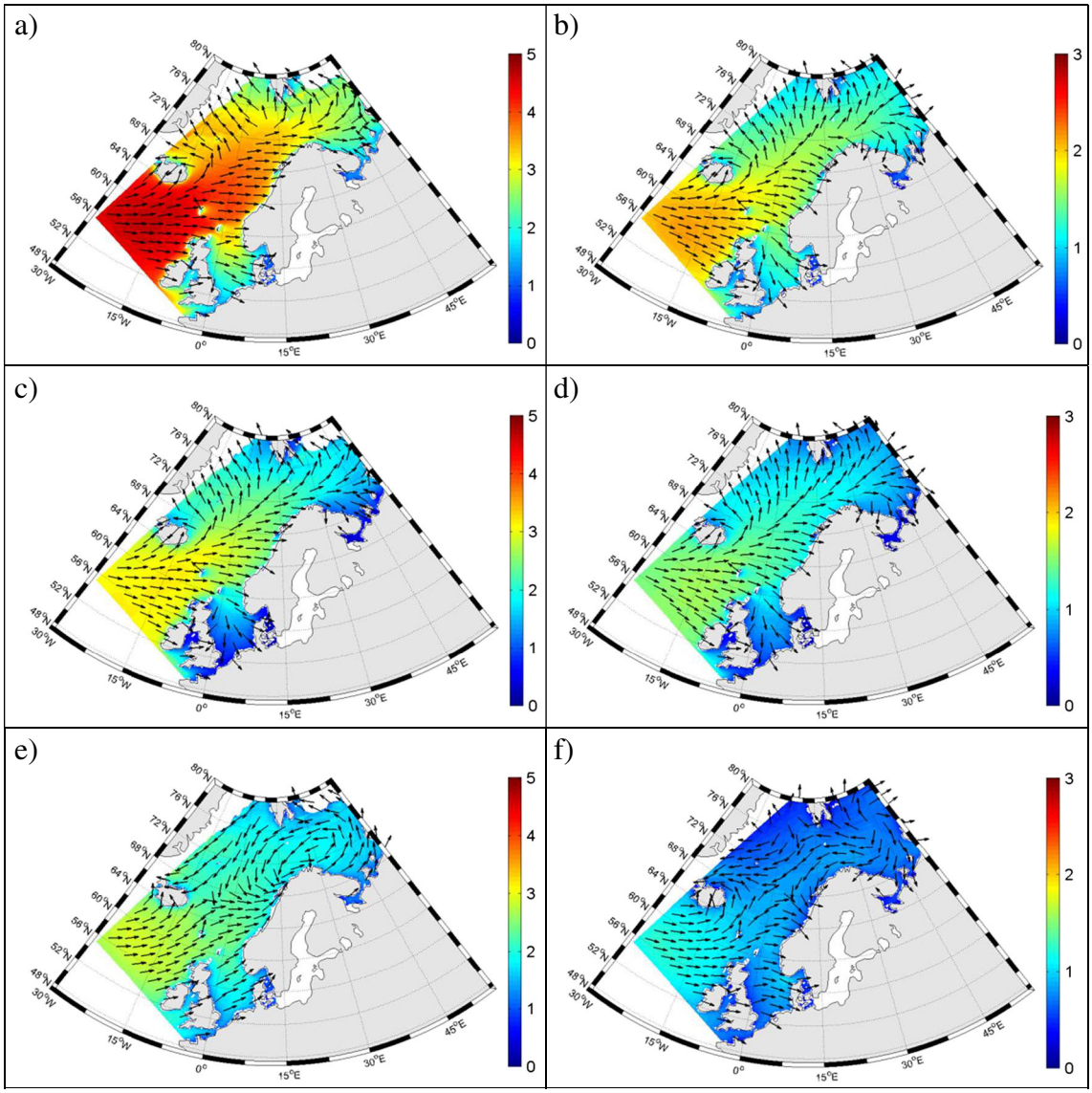

Fig. 2 Seasonal averages of $H_s(m)$ for **a** DJF and **b** JJA, of $H_S^S(m)$ for **c** DJF and **d** JJA, and of $H_S^W(m)$ for **e** DJF and **f** JJA, as well as θ_m (°), θ_m^s (°), and θ_m^s (°) for the corresponding seasons. The *arrows* are not scaled with the background fields, and the *color scales* vary between the DJF and JJA panels

In Semedo et al. (2011a), it was shown that in the open ocean, even in the main wave generation areas along the extratropical storms tracks, swell-dominated wave fields are predominant, with frequencies of occurrence higher than 75 % in most areas, and close to 100 % in the tropical band. Due to lower resolution, the details of the swell predominance in the Nordic Seas (and in other coastal or semi-enclosed areas) were not very clear in Semedo et al. (2011a, their Fig. 6.), although showing in most cases frequencies of occurrence of swell-dominated wave fields of the order of 75 % in the winter and higher than 85 % in the summer. The DJF and JJA spatial distributions of P_s , here presented with additional detail, can be seen in Fig. 4. In both seasons, the frequencies of occurrence of swell-dominated wave fields have higher values in the Norwegian Sea, compared to other areas of the domain. Lower predominance of swell waves can be seen in the North and Barents Seas, which can roughly be linked to the wind speed and to the wind sea and swell wave heights pattern shown in Figs. 1 and 2, respectively, and to the fetch length in those areas. In the Norwegian Sea, the values of P_s are around 70–75 % in winter, and in JJA, these values increase to 85–90 %. In the North Sea, the probability of having a swell-dominated wave field is considerably lower: around 30–35 % in winter, and close to 60 % in summer. In the Greenland and North Seas and in Barents Sea near Svalbard, mostly in DJF, the values of P_s are low (~10–20 %). This can be explained by the sea ice effect, which was not accounted for in the computation of P_s . In some (most) winters of the 1958–2001 period, these areas were covered with ice and are looked at as "land", considerably lowering the probability of having

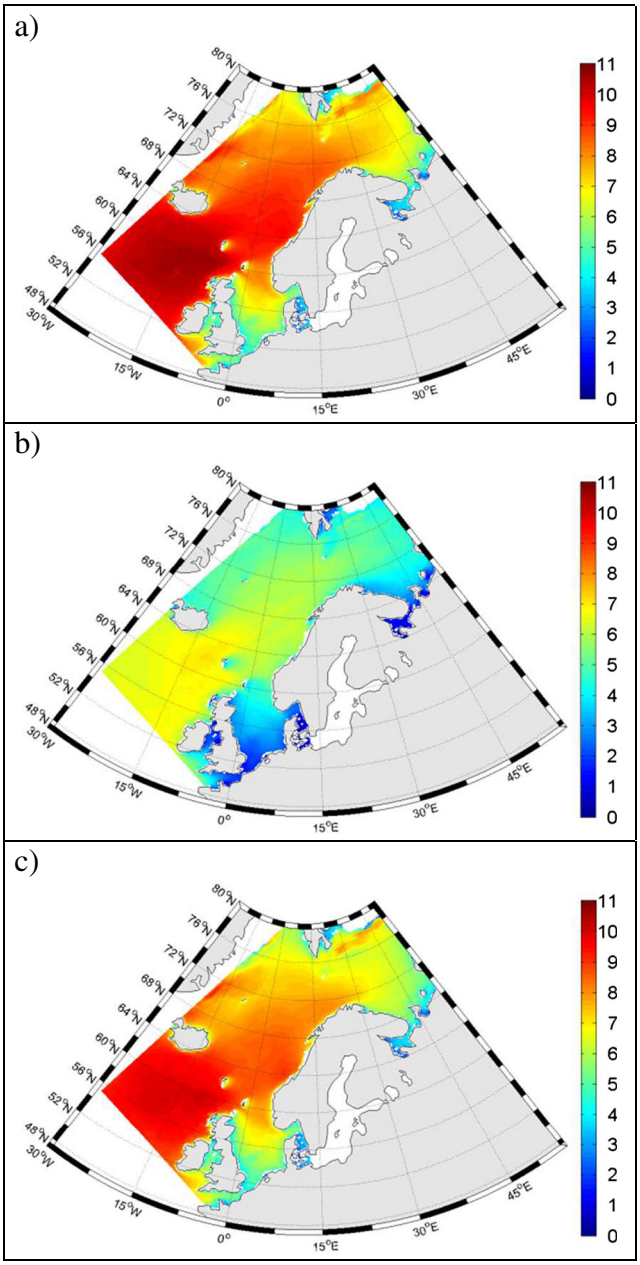

Fig. 3 Seasonal averages of the DJF 99 % percentile of **a** $H_s(m)$, **b** of $H_S^S(m)$, and **c** of $H_S^W(m)$

swell waves in the area, since we are computing the frequency of occurrence for the whole period. The sea ice poses specific challenges to wave climate studies in high latitudes (Tuomi et al. 2011) that are not considered here, since this is out of the scope of this study, and by taking it into account, it would mask the results in the open sea areas.

According to the wave growth theory, U_{10} and H_s follow a monotonic relationship at the growing (wind sea) state (Holthuijsen 2007) up to the fully developed spectrum or saturation level. The equilibrium between wind and waves can be seen as an asymptotic state where the wave spectrum is fully developed, and from then on, the shape of the spectrum and the peak frequency are only changing slowly in time. The wave age can therefore also be seen as a measurement of this equilibrium state at its asymptotic values $c_p/U_{10} = 1.2$ (Pierson and Moskowitz 1964; Alves et al. 2003). The probability (frequency of occurrence) of having a fully developed sea state in the area of interest, i.e., $P\left[c_p/U_{10} = 1.2 \pm 0.025\right]$, has been computed (not shown) and it is very low (~4–5 %, although slightly higher in DJF in the Northern Sea). This means that the Nordic Seas are most of the time in a state of non-equilibrium, i.e., waves are either growing or propagating away from their generating area.

Figure 5 shows the DJF scatter diagrams of U_{10} and H_s for five positions (closest grid point to in situ wave height observations sites at three of these positions) represented in the map in the same figure. The U_{10} and H_s follow the empirical relation between significant wave height and wind speed from Pierson and Moskowitz (1964), further corrected by Alves et al. (2003), where

$$H_s = 0.02U_1 0^2. \tag{4}$$

The color density in the scatter plots depicts the data density normalized by the maximum values, and the overlaid curves in red correspond to the fully developed sea states represented by Eq. 4. The fully developed line can be seen as a separation between the wind sea and swell sea states, in a sense that values below (above) the line represent wind sea (swell) dominated sea states, i.e., with wave ages lower (higher) than 1.2. The high level of scattering showing a departure from the red curves indicates the non-equilibrium state mentioned above. This high scattering can be partially explained by the wind regime in these areas, where frontal weather with different tracks generating high waves alternates with high pressure systems with calm winds. Nevertheless, this ocean feature is common in the world ocean, where fully developed sea states with an equilibrium between the waves and atmosphere (winds) are also uncommon (Semedo 2010). A more careful look shows that in winter in the North Sea (NS-62123), the scattering is somehow lower and that more growing wind seas take place, compared to the other positions. A different situation occurs at the open-ocean positions (NA and NW1-64045), located along the Norwegian Sea axis, where storms and swell propagate preferably (see Figs. 1 and 2). There, the scattering is higher than in the North Sea, and now, the swell predominance is also higher, with a higher density of points above the equilibrium line. A transition situation occurs at the position NW2-63103, between the Shetland Islands and main land Norway, with a slight increase in the wind sea occurrences, compared to the open ocean, and less scattering. An additional position (BS) between the North Norwegian Sea and the Barents Sea was chosen. The situation is not substantially different from the two open-ocean

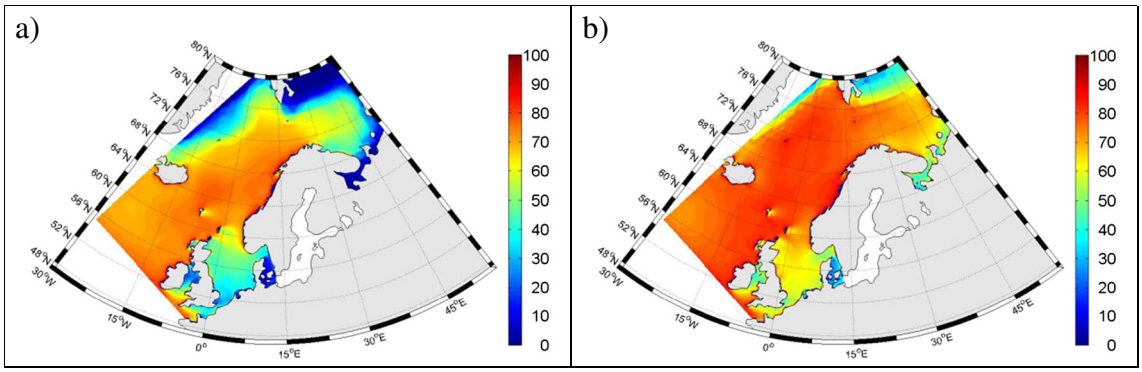

Fig. 4 Seasonal regional distribution of the swell prevalence (P_s ; dimensionless) for **a** DJF and **b** JJA

positions, since this position is also located along the swell propagation axis, and there, as seen in Fig. 4, even in the winter, swell prevails. Therefore, the highest concentration of points in the scatter diagram is also above the equilibrium line in the swell part.

Figure 2 showed that $H_s^s > H_s^w$ in the Norwegian and Greenland Seas, and $H_s^s \approx H_s^w$ in the North and Barents Seas, regardless of the seasons (in DJF and JJA, as shown, but also in MAM and SON, not shown), with the exception of JJA in the North Sea, where $H_s^s < H_s^w$. The differences between the wind sea and swell significant wave heights are, nevertheless, lower in the Nordic Seas than in the open ocean. On the other hand, swell waves, as seen in Figs. 4 and 5, are dominant or more prevalent most of the time ($P_s > 50\,\%$) in most of the Nordic Seas area in DJF and JJA (as in the intermediate seasons, not shown). Nevertheless, we need to know which type of waves carries more energy in the area. To assess the relative spectral weight of the two types of waves in the Nordic Seas, as in Semedo et al. (2011a) for the global ocean, the swell and wind sea energy densities per unit area (in Jm^{-2}) were computed: $E^s = \rho g m_0^s$ and $E^w = \rho g m_0^w$, where ρ is the water density, g is the acceleration of gravity, and m_o^s and m_o^w are the swell and wind sea zeroth moments, respectively. Figure 6 shows the DJF and JJA maps of the regional spatial distribution of the swell spectral energy proportion (weight) to the total wave energy at the surface (E^s/E , where E is the total wave spectral energy). The wind sea spectral energy proportion defined as $E^w/E = 1 - (E^s/E)$ is not shown here. It is clear that, as in the open ocean, swell waves carry most of the energy at the sea surface in the Nordic Seas, with spectral weights of 65 % and higher in the Norwegian Sea and most of the Greenland and Barents Seas, in DJF. In JJA these values are even higher, as expected, and swell waves carry 85–90 % of the energy at the surface in the same area, with the exception of lower swell energy content areas south of Iceland and in the south part of the Barents Sea. The higher resolution of NORA10, compared to ERA-40, allows the analysis of the swell spectral energy in the North Sea, where lower (higher) values of swell (wind sea) energy weight can be seen in the winter (55–60 %). In summer, swell waves carry 65–70 % of the wave energy.

3.3 Large scale atmospheric forcing

The relationship between the climatological variability of wave heights and large scale atmospheric patterns, normally represented by atmospheric indices, has been the subject of several studies. These studies have been pursuit in the North Atlantic (e.g., Bacon and Carter 1991, 1993; Bauer 2001; Wang and Swail 2001; Woolf et al. 2002) and in other ocean basins (e.g., Bromirski et al. 2005; Hemer et al. 2010, in the Pacific Ocean and in the Southern Hemisphere, respectively), mostly with the goal of trying to understand changes in the wave climate as a response to changes in the atmospheric circulation. Here, we present the relationship between H_s, H_s^s , and H_s^w and the large scale atmospheric circulation pattern as represented by the North Atlantic Oscillation (NAO) that largely explains the extratropical atmospheric circulation in the North Atlantic sub-basin, particularly in the winter (Luo et al. 2011). The NAO is a measure of the North Atlantic meridional air pressure gradient and of the strength of the prevailing westerly winds, based on the sea-level pressure difference between the Azores High and the Iceland Low (Hurrell 1995). The NAO has a strong influence on the surface marine climate (Hurrell 1996), particularly in the European/Atlantic sector, and is often referred to as a seesaw of the atmospheric sea-level pressure between the Arctic and subtropical Atlantic (Hurrell 1995). Both phases of the NAO (positive and negative) are related to the intensity and location of the North Atlantic jet stream and to the extratropical storm tracks and strength (Visbeck et al. 2001). A positive phase of the NAO corresponds to stronger-than-average westerly winds over the mid latitudes and to storm paths more to the north-eastward, towards the northern part of the North Atlantic, into the Norwegian Sea. A negative phase corresponds to weaker westerly winds, with the storm tracks more south-eastward, towards the southwest Europe, into the Iberian Peninsula (Hoskins and Hodges 2002).

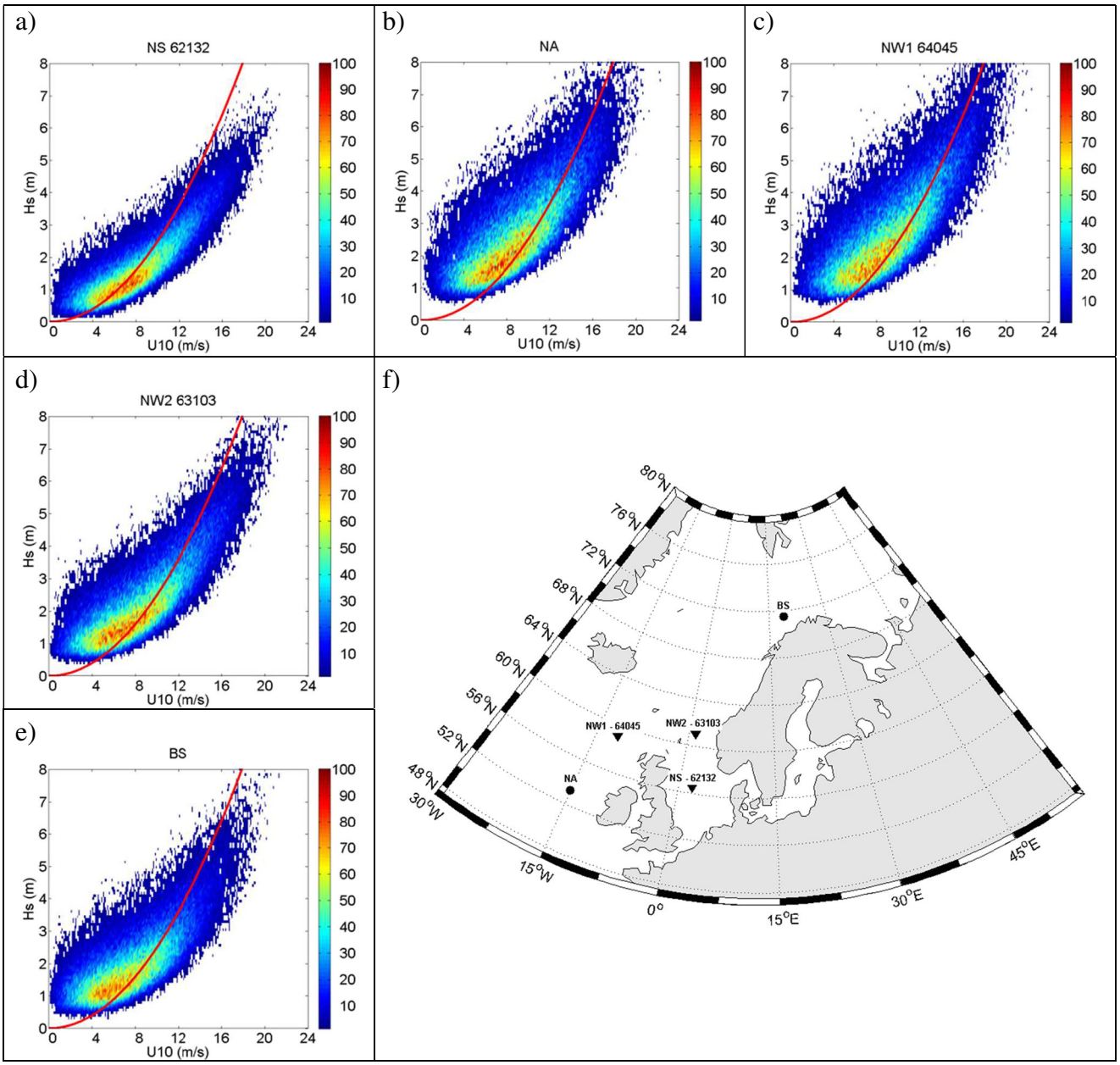

Fig. 5 Scatter diagrams of $U_{10}(ms^{-1})$ and H_s (m) for positions **a** NS-62132 (56.50N; 02.09E), **b** NA (53.20N; 15.00W), **c** NW1-64045 (59.00N; 11.50W), **d** NW2-63103 (61.10N; 01.10E), and **e** BS (71.50N; 19.00E) for DJF, and **f** map with the previous positions. The *overlaid red lines* represent the Pierson and Moskowitz relation between U_{10} and H_s for fully developed seas shown in Eq. 4

Figure 7 shows the DJF correlation maps (r -correlation coefficient) between H_s, H_s^s , and H_s^w and the NAO index, where additional detail from the higher resolution of the NORA10 wave data is provided. The correlations in JJA are not shown because they are not relevant, since the effect of the NAO on the North Atlantic sub-basin wave field is mostly a winter phenomena (Bauer 2001). During summer, particularly close to the coast, mesoscale wind features, like sea breezes or coastal low-level jets (Ranjha et al. 2013; Soares et al. 2014), for example, are more relevant in the definition of the regional wave climate characteristics, since the Westerlies and the extratropical storms are weaker (see Fig. 1 above and Fig. 1 in Semedo et al. 2011a). The correlation values between H_s and the NAO are high ($r\approx 0.8$) near the west coast of Ireland, and relatively high ($r\gtrsim 0.7$) in a large area towards the Norwegian Sea, but lower again in the North Sea ($r\lesssim 0.5$), where the sheltering effect of Great Britain is noticeable. The correlation is also low in the Barents Sea ($r\lesssim 0.3$). The correlation patterns between H_s^s and H_s^w and the NAO are different, and the propagation effect of swell and the local generation of wind sea waves are clear. The correlation coefficient of swell waves and the NAO is ~0.7 in a larger area of the domain,

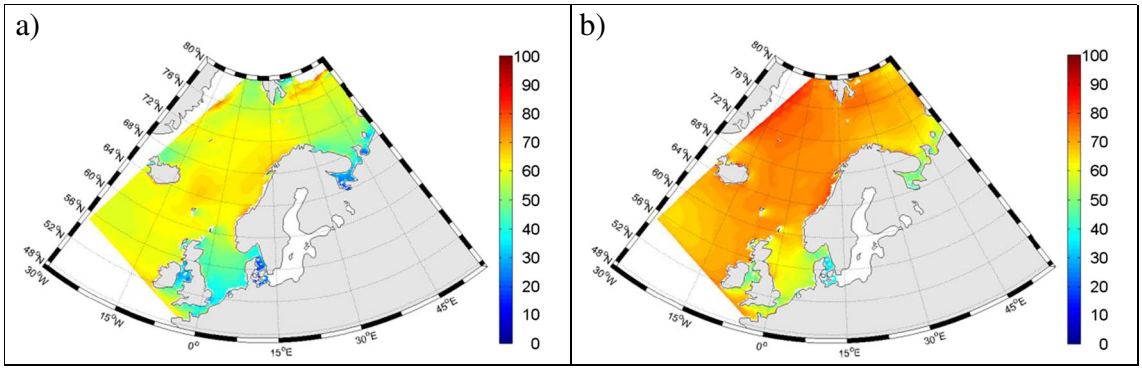

Fig. 6 Seasonal regional distribution of the swell energy weight (dimensionless) for **a** DJF and **b** JJA

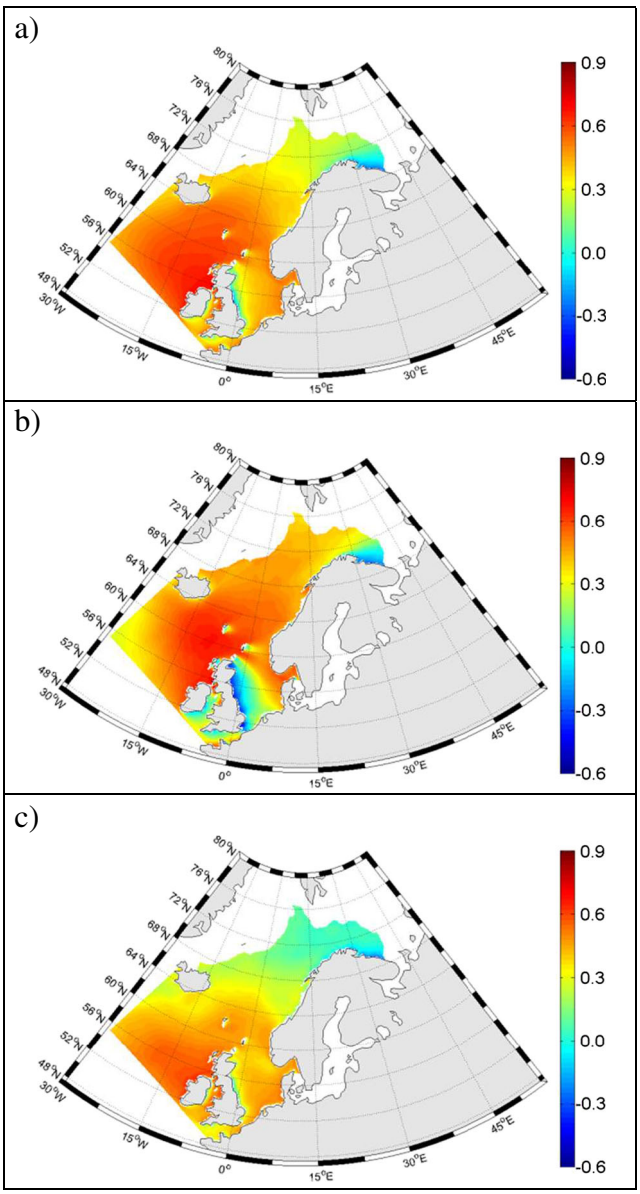

Fig. 7 Seasonal correlations (dimensionless) of the DJF **a** H_s with NAO, **b** H_s^s with NAO, and **c** H_s^w with NAO

between the British Islands and Iceland, and into the Norwegian Sea, with a considerably lower correlation in the North Sea due to a strong sheltering effect. The correlation coefficients between the H_s^w and the NAO are lower, with a peak area south of Iceland ($r \approx 0.55$), where the Westerlies blow strongest in DJF (see Fig. 1). The wind sea waves are practically uncorrelated with the NAO in the north part of the Norwegian Sea, reaching values close to zero in the Barents Sea. The higher correlation values of the swell wave heights with the NAO in the north part of the Norwegian Sea and in the Barents Seas (not seen in ERA-40 due to the coarser resolution; Semedo et al. 2011a), along with the sheltering effect in the North Sea, can be seen as an indicator of waves generated more south that propagated north-westward. Since the NAO is strongly related to the strength of the zonal atmospheric flow and to the extratropical storm tracks in the North Atlantic sub-basin (Hurrell 1996), the impact of its positive and negative phases, separately, on the winter H_s, H_s^s, and H_s^w climates in the Nordic Seas are investigated. The total, swell, and wind sea significant wave heights patterns are investigated using the phase of the NAO index as the separation criterion between the northeast and southeast orientation of the storm tracks. The winter H_s, H_s^s, and H_s^w climatological means were computed separately for positive and negative NAO events (NAO^+ and NAO^-, respectively). The DJF H_s, H_s^s, and H_s^w NAO^+ and NAO^- climatological means are shown in Fig. 8. The differences between the effects of the positive and negative NAO regimes, and of the different atmospheric circulation patterns they entail, on the wave heights in the North Eastern Atlantic wave patterns are clear.

From the DJF mean NAO^+ H_s, H_s^s, and H_s^w patterns, it can be seen that there is an overall positive departure from the correspondent winter climatological means shown in Fig. 2. The impact of higher wind speeds and (more pole-ward) storm tracks with longer fetches, characteristic of the positive NAO index regime, gives rise to higher mean H_s (~1 m higher south of Iceland), with small changes in the sheltered North Sea and east Barents Sea. Changes in the mean H_s^s can also be seen, even in the North Sea, due to the more northern storm

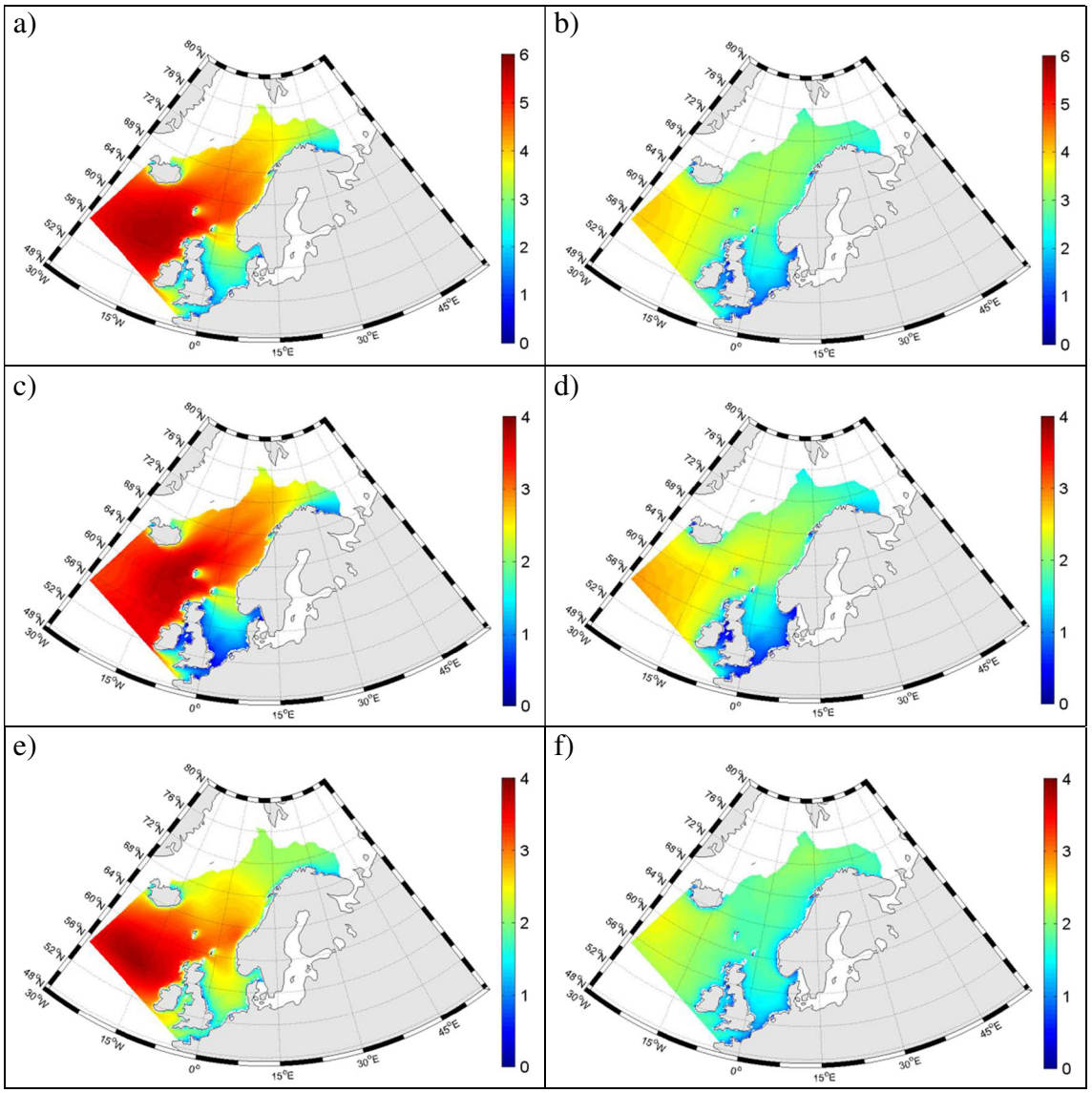

Fig. 8 Seasonal averages of $H_s(m)$ for the **a** NAO^+ and **b** NAO^- regimes, of $H_s^s(m)$ for the **c** NAO^+ and **b** NAO^- regimes, and of $H_s^w(m)$ for the **e** NAO^+ and **f** NAO^- regimes. The color scales vary between the panels

tracks and to the intrusion of swell waves in that sea. The changes in the DJF mean NAO^+ mean H_s^w are more pronounced (in percentage), with higher locally generated wave heights south of Iceland (~1 m higher, corresponding to about 25 %), but also in the northern part of the Norwegian Sea with an increase from 30 to 40 %, which can also be justified with the more pole-ward storm tracks. The DJF mean NAO^- H_s, H_s^s, and H_s^w patterns are not totally symmetric to the ones shown for the NAO^+ regime. Wind speeds are now lower in the area of interest, but in this situation, storms are tracking more to the southeast, giving rise to changes in the wave heights but also in the sea state patterns compared to the DJF climatological mean showed above. A general decrease of wave heights and a westward shift (to the outside of the domain) of the wave heights maxima (in all three analyzed parameters) can be seen. The mean H_s are lower in the entire domain, including in the North Sea. The changes in the mean H_s^s pattern along the Norwegian Sea axis, although not very high, show that there is now a lower intrusion of swell waves in that sea. The DJF NAO^- mean H_s^w also shows lower locally generated wave heights, compatible with lower wind speeds in this area during the negative phase of the NAO, although the decrease (in percentage), compared to the total DJF mean, is not as high as the increase in the H_s^w NAO^+ regime.

The swell dominance of the wave field (P_s pattern) for the NAO^+ and the NAO^- regimes (not shown) is also different, revealing a lower (higher) occurrence of swell-dominated wave fields in the Nordic Seas in the positive (negative) NAO regime, compared to the total P_s as shown in Fig. 4.

4 Long-term variability analysis

Wave observations (in situ, visual and remote sensing), re-analysis and hindcasts have shown that wave heights in the North Atlantic sub-basin have increased during the last 25–30 years of the twentieth century (see e.g., WASA Group 1998; Wang and Swail 2001; Vikebø et al. 2003, and Gulev and Grigorieva 2004), as part of a global positive wave heights trend (Sterl and Caires 2005; Hemer et al. 2010). This global wave height increase, since the early 1970s, can be linked to an increase in the global U_{10} (Sterl and Caires 2005; Semedo et al. 2013), although, due to the wave propagation effect, that link might not be exactly true everywhere. The increase in U_{10} in the North Atlantic sub-basin, particularly during winter, has been linked to an increase in the strength of the North Atlantic Westerlies, partially explained by an increase in the NAO index (WASA Group 1998). Since the area of interest in this study covers the preferred storm path in the North Atlantic, with the longest axis (fetch) along that path, the long-term winter variability of H_s^s, and H_s^w are investigated separately, to assess how they combine to influence the long-term trends of the H_s in the Nordic Seas.

Maps of the H_s, H_s^s, and H_s^w DJF linear trends for the NORA10 period in the Nordic Seas are shown in Fig. 9. The linear trends in JJA are not shown because they are close to zero and are not statistically significant. The decadal trends of H_s^s show that the largest winter upward changes from 1958 to 2001 occurred in the Norwegian Sea, with height increases of the order of 10 cm decade^{-1} or more. The swell height changes in the area southwest of Iceland, where the winter climatological wave height maxima is located, are negligible, and a decrease (around 3 cm decade^{-1}) in swell heights took place in the western part of the North Sea. As seen above, in this area, swell waves are, to a certain extent, not so high or are less prevalent during winter (see Figs. 2 and 4 above), due to the sheltering effect and to the short fetch of the predominant southwestern wind direction. The winter decadal trends pattern of H_s^w is different from the swell one, and a consistent increase in wind sea wave heights can be seen throughout the Nordic Seas (with the exception of marginal decreases in the Barents Sea), that are well correlated with very similar U_{10} decadal trends (not shown). The highest positive trends are located southwest of Iceland (>12 cm decade^{-1}), west of Ireland, Scotland, and Norway. A generalized increase of wind sea heights (7–8 cm decade^{-1}) also occurred in the North Sea. The total decadal variation of the winter H_s, as a combination of the long-term variations of H_s^s, and H_s^w, show that the increase was higher (~15 cm decade^{-1}) west of Ireland and Scotland, mostly due to wind seas (therefore, to the local wind speed increase), and along the west coast of Norway, here mostly due to the swell propagation effect. The winter H_s increased about 7–8 cm decade^{-1} in the North Sea, also mostly due to increases in wind sea waves. The spatial

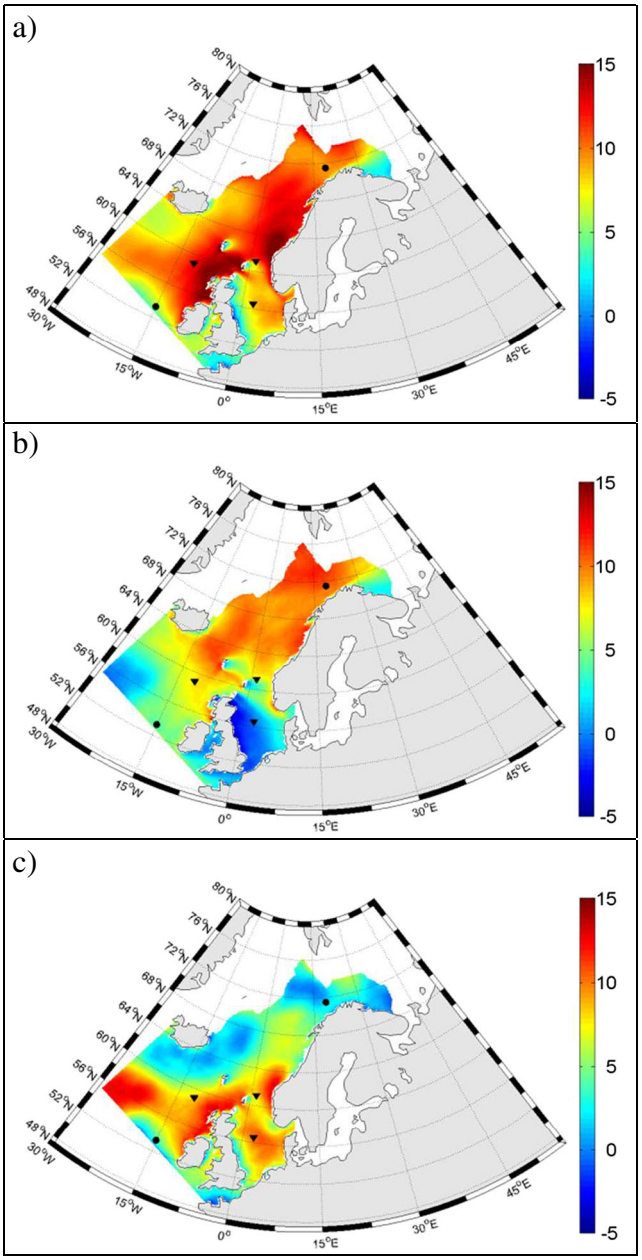

Fig. 9 Linear trends (cm decade^{-1}) in DJF of **a** H_s (*m*), **b** H_s^s, and **c** H_s^w. Positions as in Fig. 5, with *inverted triangles* (*dots*) representing positions with (without) in situ observations

patterns of the H_s^s and H_s^w linear trends are less consistent with each other in the Nordic seas than in the open ocean for the North Atlantic sub-basin. A possible explanation for this difference, as pointed out by Gulev and Grigorieva (2006) and Semedo et al. (2011a), is that the swell propagation effect towards the northeast, away from the areas of highest wind sea changes, results in a pattern of shifted swell heights variability in the central and north Norwegian Sea.

Figure 10 displays the DJF time series of the seasonally averaged values of H_s, H_s^s, and H_s^w for the five positions showed above on the map in Fig. 5, and also in Fig. 9 (for

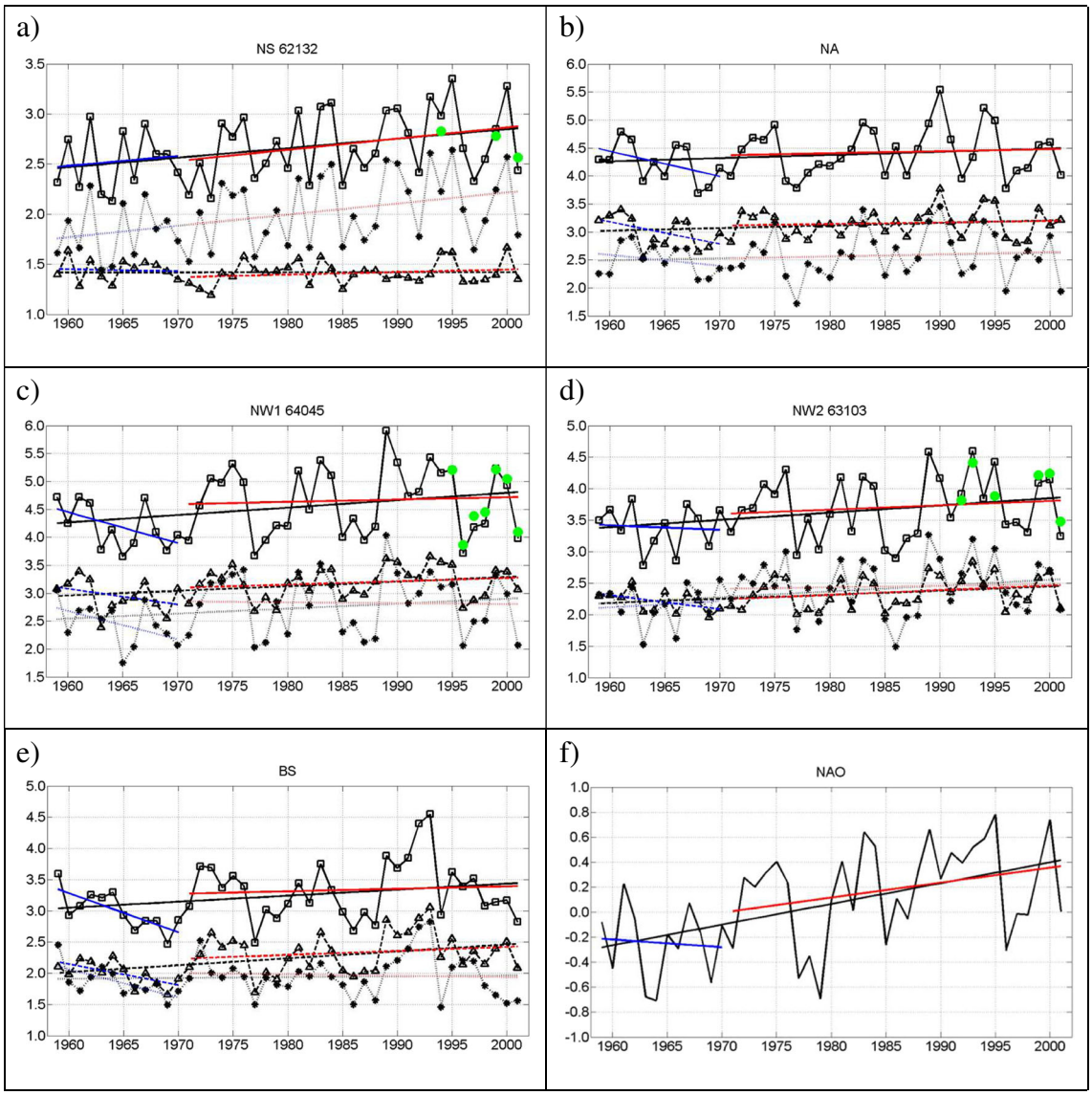

Fig. 10 Time series (*black lines*) of the mean DJF H_s (*full lines with squares*), H_s^s (*dashed lines with triangles*), and H_s^w (*dotted lines with stars*), for positions **a** NS-62132, **b** NA, **c** NW1-64045, **d** NW2-63103, and **e** BS (geographic positions in the map and caption in Fig. 5), and **f** time series of the DJF NAO index. H_s , H_s^s , and H_s^w linear trends for 1958–2001 (*black full*, *dashed*, and *dotted lines*, respectively), 1958–1970 (*blue full*, *dashed*, and *dotted lines*, respectively), and 1971–2001 (*red full*, *dashed*, and *dotted lines*, respectively). NAO index linear trends for 1958–2001 (*black full line*), for 1958–1970 (*blue full line*), and for 1971–2001 (*red full line*). Buoy observations (H_s ; DJF means) as *green dots*

convenience, allowing a spatial comparison between the five positions). The DJF NAO index time series is also shown in Fig. 10. The linear trends of H_s, H_s^s , and H_s^w at these five positions are also shown. Although the scope of the present study is not the validation of the NORA10 wave data (that has been done by Reistad et al. 2011), buoy observations of H_s are overlaid in the time series shown in Fig. 10 (only in three of these positions, and for which the buoy code is in the position label; see Fig. 5). The good agreement between measured and modeled DJF H_s gives us confidence in the ability of NORA10 to simulate realistic decadal trends.

The linear trends in Fig. 10 were computed for three different periods: for the whole NORA10 period (1958–2001), and for two partial periods, from 1958 to 1970 and from 1971 to 2001 (henceforth called period 1 and period 2, respectively), when generalized decreases and increases of wave heights, respectively, occurred in the North Atlantic sub-basin (Bauer et al. 1997; WASA Group 1998; Bauer 2001). The mean winter NAO index, and the correspondent linear trends for 1958–2001 and for periods 1 and 2, is also shown. The statistically significant yearly H_s, H_s^s , and H_s^w winter trends (nominal and in %), for the three periods, are

shown in Table 1. With the exception of the position in the North Sea, the mean winter H_s^s is always higher than the H_s^w one, as expected, regarding what was shown above. At all positions, with the exception of NS-62138, the mean winter H_s decreased from 1958 to 1970, and from then on, it increased consistently until 2001.

The H_s winter trend in the North Sea is 0.95 % yr^{-1} for the all period, during which the DJF mean H_s increased by 10.8 cm. This increase is driven totally by H_s^w, which has increased by 1.1 % yr^{-1} (12.7 cm), while swell wave heights remained practically unchanged from 1958 to 2001. Similar trends can be seen for period 1 in NS-62138, although in this case, H_s^s actually decreased (slightly) during periods 1. At NA (west of Ireland), the H_s winter trend is also positive for the whole period (0.95 % yr^{-1}, corresponding to an increase of 23.9 cm), although during period 1, the mean winter H_s actually decreased (4.47 % yr^{-1}, −49.2 cm in total), due to the combined effect of negative trends of wind sea and swell waves. In period 2, the H_s, H_s^s, and H_s^w trends at NA are all positive. Slightly further north, at the NW1-64045 and NW2-63103 positions, the trends are similar, although more defined in the former, where in the full period H_s increased 1.33 % yr^{-1} (55.9 cm), with similar positive trends for H_s^s, and H_s^w (0.82 and 0.89 % yr^{-1}, corresponding to a total increase of 34.5 and 37.3 cm, respectively). During period 1, the H_s, H_s^s, and H_s^w trends at NW1-64045 are all negative, following similar trends as at the NA position in open ocean. In the same period, the trends at NW2-63103 are slightly more complex, since the sheltering effect from the British Isles and the Shetland Isles influences the swell propagation and the fetch dimensions (see prevailing winter wind direction and swell and wind sea mean directions above in Figs. 1 and 2, respectively). At this position, the mean winter H_s and H_s^s decreased by 7.8 and 24.5 cm, respectively (−0.7 and −2.23 % yr^{-1}, respectively) during the whole period, while H_s^w actually increased 10.8 cm (0.98 % yr^{-1}). During period 2 at both NW1-64045 and NW2-63103, the trends are positive for the total, swell, and wind sea significant wave heights. The trends at these positions, with the exception of the one in the North Sea, coincide with an increasing NAO index period from 2059 to 2001, and with a decreasing (increasing) NAO index in period 1 (period 2).

At the BS position entering the Barents Sea, at the north edge of the domain, positive trends of the mean winter H_s, during the full period occurred. The decrease in the winter mean H_s during period 1 was the largest of the five positions (6.29 % yr^{-1}, corresponding to a decrease of almost 70 cm). During period 2, the winter mean H_s increased by 11.9 cm (0.4 % yr^{-1}) due to remotely generated waves (H_s^s increased by 19.0 cm, at 0.63 % yr^{-1}), since the wind sea wave heights decreased 6.4 cm (−0.21 % yr^{-1}).

5 Summary and conclusions

A qualitative analysis of the wave field in the Nordic Seas, from the high-resolution regional reanalysis NORA10, has been presented. The analysis is done for wind sea and swell

Table 1 Total (in cm) and yearly (in % inside the curly brackets) long-term variability of the DJF H_s H_s^s and H_s^w for the periods 1958–1970 and 1971–2001 and for the all period (1958–2001)

1958–1970 cm (%)			
	H_s	H_s^s	H_s^w
NS-62132	10.8(0.98)[a]	−2.1(−0.19)[c]	12.7(1.16)[b]
NA	−49.2(−4.47)[a]	−43.5(−3.96)[a]	−21.1(−1.92)[a]
NW1-64045	−61.2(−5.56)[a]	−30.9(−2.81)[a]	−55.8(−5.07)[a]
NW2-63103	−7.8(−0.70)[a]	−24.5(−2.23)[b]	10.8(−0.98)[a]
BS	−69.2(−6.29)[a]	−37.4(−3.40)[a]	−50.0(−4.54)[a]
1971–2001 cm (%)			
NS-62132	33.4(1.11)[a]	7.6(0.25)[a]	32.8(1.09)[a]
NA	11.1(0.37)[a]	8.4(0.28)[a]	11.8(0.39)[a]
NW1-64045	12.6(0.42)[a]	17.8(0.59)[a]	−4.9(−0.16)[b]
NW2-63103	20.7(0.69)[a]	22.1(0.74)[b]	7.2(0.24)[b]
BS	11.9(0.40)[a]	19.0(0.63)[b]	−6.4(−0.21)[b]
1958–2001 cm (%)			
NS-62132	39.9(0.95)[a]	0.3(0.01)[b]	46.8(1.11)[a]
NA	23.9(0.57)[a]	19.2(0.46)[a]	14.3(0.34)[c]
NW1-64045	55.9(1.33)[a]	34.5(0.82)[a]	37.3(0.89)[a]
NW2-63103	48.2(1.15)[a]	27.2(0.65)[a]	38.7(0.92)[a]
BS	40.3(0.96)[a]	46.4(1.10)[a]	5.4(0.13)[b]

[a] Significant at the 99 % level

[b] Significant at the 95 % level

[c] Significant at the 90 % level

waves separately, based on the premise that the simple study of SWH and MWP give a limited description of the sea state, and therefore, a more detailed investigation from a qualitative stand point is needed to correctly define the wave field characteristics and climate of a certain area. The higher resolution of the NORA10 (winds and waves), along with the bottom friction effect, allowed a better description of the wind sea and swell features in the Nordic Seas, compared to previous global studies, e.g., the one from Semedo et al. (2011a). Finer resolution resolves local and stronger winds better, as well as the impact of the coastline on the wind field, leading to a better representation of the waves (as shown in Reistad et al. 2011), and therefore to a better representation of the regional wind sea and swell fields.

The long-term variability of the wind sea and swell significant wave heights were investigate separately to assess how they combine to influence the long-term trends of the SWH in the Nordic Seas. The influence of the large scale atmospheric circulation patterns, represented by the NAO index on the wind sea and swell regional climates has also been investigated.

It has been shown that the wind sea and swell characteristics in the Nordic Seas are different from the open ocean, where the mean H_s^s , is clearly higher than the mean H_s^w . This is not exactly the case in the Nordic Seas, mainly in the North and Barents Seas, where swell waves are less predominant and H_s^s is comparable or lower than H_s^w . This occurs due to the sheltering effect and to the orientation of the fetch in relation to the coast lines and to the mean wind direction. The coastal geometry, compared to the prevailing wave and wind propagating directions, plays a very important role in the definition of the wind sea and swell climates in the Nordic Seas. In the growing process, waves require sufficient time and room for the wind to act on the ocean surface, and for the waves to propagate away for their generation area. Here, we have shown that when the fetch is limited or when sheltering occurs, wave heights are lower and the swell (wind sea) prevalence is lower (higher). That is the case (mainly) in the North Sea during winter, where the mean H_s^w can be higher than the H_s^s one. Nevertheless, swell waves are clearly more prevalent in most areas of the Nordic Seas and carry most of the energy at the ocean surface, although less than in the open ocean. That is not the case during extreme wave heights events, since in this situation, when the ocean surface is under severe stormy weather and high wind speeds are present, the climatological mean H_s^w is higher than the mean H_s^s .

The impact of storm tracks and strength of the zonal flow (represented in the present study by the NAO index) on the wave fields were investigated. The DJF H_s, H_s^s , and H_s^w climatological means were computed for the corresponding NAO^+ and NAO^- periods from 1958 to 2001, and the influence of the storm track patterns in the Nordic Sea wave climate was shown to be clear, not only on the SWH magnitude, but also on the relation between the wind sea and swell heights. On the one hand, during NAO^+ events, when the Westerlies are stronger and storms track more northerly, the mean winter H_s is higher in the Nordic seas, and the H_s^s and H_s^w are comparable in most areas but not in the north Norwegian Sea and in the Barents sea, due to swell propagation. On the other hand, during NAO^- events, winds in the Nordic Seas are weaker as storms propagate more southward. Hence, the mean H_s^s is higher than the H_s^w one in almost all parts of the Nordic Seas, and swell waves are more prevalent (not shown) and carry more energy (not shown).

Large changes in the wintertime atmospheric circulation over the North Atlantic during the NORA10 period (Hurrell and Van Loon 1997; Weisse et al. 2005) had an impact on the wave heights, mostly in the eastern North Atlantic mid to high latitudes (Bacon and Carter 1991, 1993). From the early 1940s until the early 1970s, the NAO index exhibited a downward trend, which can be seen (from 1958 onwards) on Fig. 10. After ~1971 until the end of the 20th century, a sharp reversal has occurred, and the NAO index increased, and remained mostly positive, with highly-positive values after 1980. The decadal trends of the wintertime H_s shown in Fig. 9, and particularly in four of the five positions in Fig. 10 (the exception being NS-62132 in the North Sea) follow the mean winter NAO phase trends, clearly suggesting that the decrease (increase) in period 1 (period 2) are strongly related to the large scale atmospheric circulation pattern. The way H_s^s , and H_s^w combine in defining the H_s long-term trends reveal that in the open ocean, the increases/decreases can be attributed mostly to swell and to the wave propagation effect. That is not the case in the North Sea, where the limited fetch effect plays a significant role.

ERA-40 suffers from inhomogeneities, mostly due to changes in observing systems used in the assimilated observations. Four distinctive periods are identified in Sterl and Caires (2005). Although these periods are not coincident with periods 1 and 2 mentioned in section 4, the possibility that inhomogeneities have propagated to NORA10 and are responsible for the abrupt change of the wave heights between these periods should not be ruled out. Nevertheless, the agreement between H_s and the NAO trends is striking, supporting the conclusion that these trends are related to the large scale atmospheric circulation. The assessment of the propagation of the ERA-40 inhomogeneities into the NORA10 and how they might affect wave heights decadal trends is beyond the scope of the present study, but should be investigated in future research. An additional matter that can be further investigated is the effect of finer resolution of wind fields on the wind sea and swell representations.

Waves play a significant role on the global climate system and have been included in many assessments of climate, including the latest Intergovernmental Panel on Climate Change (IPCC) fifth assessment report (AR5; IPCC 2013).

Although several global dynamic wave climate projections towards the end of the twenty-first century (e.g., Dobrynin et al. 2012; Fan et al. 2013; Hemer et al. 2013; Semedo et al. 2013) have been published in the scientific literature, a more detailed qualitative look on the impact of climate change on regional wind sea and swell climates needs to be pursuit.

Acknowledgments Alvaro Semedo's work was done in the framework of the SHARE and CLIBECO projects, financed by the Portuguese Foundation for Science and Technology (FCT - *Fundação para a Ciência e Tecnologia*, Portugal). Roberto Vettor's work was supported by the FCT under the contract no. SFRH/BD/89476/2012. Øyvind Breivik's contribution was supported through the European Union FP7 project MyWave (grant no 284455), while the Norwegian Deepwater Programme is acknowledged for its support of his work on the construction of the NORA10 archive. C. Guedes Soares' contribution was also made in the scope of the CLIBECO project.

References

Aarnes OJ, Breivik Ø, Reistad M (2012) Wave extremes in the northeast Atlantic. J Clim 25:1529–1543

Alves JHGM (2006) Numerical modeling of ocean swell contributions to the global wind-wave climate. Ocean Model 11:98–122

Alves JH, Banner ML, Young IR (2003) Revisiting the Pierson-Moskowitz asymptotic limits for fully developed wind waves. J Phys Oceanogr 33:1301–1323

Ardhuin F, Jenkins A (2006) On the interaction of surface waves and upper ocean turbulence. J Phys Oceanogr 33:551–557

Ardhuin F, Chapron B, Collard F (2009) Observation of swell dissipation across oceans. Geophys Res Lett 36, L06607. doi:10.1029/2008GL037030

Bacon S, Carter DJT (1991) Wave climate changes in the North Atlantic and North Sea. Int J Climatol 11:545–558

Bacon S, Carter DJT (1993) A connection between mean wave height and atmospheric pressure gradient in the North Atlantic. Int J Climatol 13:423–436

Bauer E (2001) Interannual changes of the ocean wave variability in the North Atlantic and in the North Sea. Clim Res 18:63–69

Bauer E, Stolley M, Von Storch H (1997) On the response of surface waves to accelerating the wind forcing. GKSS Manuscript 96/E/89, 24 pp

Belcher S, Grant ALM, Hanley K, Fox-Kemper B, Van Roekel L, Sullivan P, Large W, Brown A, Hines A, Calvert D, Rutgersson A, Pettersson H, Bidlot J, Janssen P, Polton J (2012) A global perspective on Langmuir turbulence in the ocean surface boundary layer. Geophys Res Lett 39, L18605. doi:10.1029/2012GL052932

Bengtsson L, Hodges K, Roeckner E (2006) Storm tracks and climate change. J Clim 19:3518–3543

Bidlot J-R (2001) ECMWF wave model products. ECMWF Newsletter, No. 91, ECMWF, Reading, United Kingdom, p 9–15

Bidlot J-R, Holmes D, Wittmann P, Lalbeharry R, Chen H (2002) Intercomparison of the performance of operational ocean wave forecasting systems with buoy data. Weather Forecast 17(2):287–310

Bosserelle C, Pattiaratchi C, Haigh I (2011) Inter-annual variability and longer-term changes in the wave climate of Western Australia between 1970 and 2009. Ocean Dyn. doi:10.1007/s10236-011-0487-3

Breivik Ø, Gusdal Y, Furevik BR, Aarnes J, Reistad M (2009) Nearshore wave forecasting and hindcasting by dynamical and statistical downscaling. J Mar Syst 78(2):S235–S243. doi:10.1016/j.jmarsys.2009.01.025

Breivik Ø, Aarnes J, Bidlot J-R, Carrasco A, Saetra Ø (2013) Wave extremes in the North East Atlantic from ensemble forecasts. J Clim 26:7525–7540

Bromirski PD, Cayan DR, Flick RE (2005) Wave spectral energy variability in the northeast Pacific. J Geophys Res 110, C03005. doi:10.1029/2004JC002398

Cavaleri L, Fox-Kemper B, Hemer M (2012) Wind waves in the coupled climate system. Bull Am Meteorol Soc 93:1651–1661

Chang EKM, Lee S, Swanson KL (2002) Storm track dynamics. J Clim 15:2163–2183

Charnock H (1955) Wind stress on a water surface. Q J R Meteorol Soc 81:639–640

Charnock H (1958) A note on empirical wind-wave formulae. Q J R Meteorol Soc 84:443–447

Chawla A, Spindler DM, Tolman HL (2012) Validation of a thirty year wave hindcast using the Climate Forecast System Reanalysis winds. Ocean Model 70:189–206

Chen G, Chapron B, Ezraty R, Vandemark D (2002) A global view of swell and wind sea climate in the ocean by satellite altimeter and scatterometer. J Atmos Ocean Technol 19:1849–1859

Csanady GT (2003) Air-Sea Interaction: Laws and Mechanisms. Cambridge University Press, Cambridge, p 248

Dobrynin M, Murawsky J, Yang S (2012) Evolution of the global wind wave climate in CMIP5 experiments. Geophys Res Lett 39:L18606. doi:10.1029/2012GL052843

Fan Y, Lin S-J, Held IM, Yu Z, Tolman HL (2012) Global ocean surface wave simulation using a coupled atmosphere-wave model. J Clim 25:6233–6252

Fan Y, Held IM, Lin S-J, Wang X (2013) Ocean warming effect on surface gravity wave climate change for the end of the 21st 701 century. J Clim 26:702, No. 16, 6046–6066

Fan Y, Lin S-J, Griffies SM, Hemer MA (2014) Simulated Global Swell and Wind Sea Climate and Their responses to Anthropogenic Climate Change at the End of the 21st Century. J Climate 27:3516–3536

Gerling TW (1992) Partitioning sequences and arrays of directional wave spectra into component wave systems. J Atmos Ocean Technol 9:444–458

Guedes Soares C (1984) Representation of double-peaked sea wave spectra. Ocean Eng 11(2):185–207

Gulev SK, Grigorieva V (2004) Last century changes in ocean wind wave height from global visual wave data. Geophys Res Lett 31, L24302. doi:10.1029/2004GL021040

Gulev SK, Grigorieva V (2006) Variability of the winter wind waves and swell in the North Atlantic and North Pacific as revealed by the voluntary observing ship data. J Clim 19:5667–5685

Hanley KE, Belcher SE, Sullivan PR (2010) A global climatology of wind–wave interaction. J Phys Oceanogr 40:1263–1282

Hanson JL, Phillips OM (2001) Automated analysis of ocean surface directional wave spectra. J Atmos Ocean Technol 18:277–293

Hemer MA, Church JA, Hunter JR (2010) Variability and trends in the directional wave climate of the Southern Hemisphere. Int J Climatol 30:475–491

Hemer MA, Fan Y, Mori N, Semedo A, Wang X (2013) Projected changes in wave climate from a multi-model ensemble. Nat Climate Change 3:471–476. doi:10.1038/NCLIMATE1791

Högström U, Smedman A-S, Sahleé E, Drennan WM, Kahama KK, Pettersson H, Zhang F (2009) The atmospheric boundary layer during swell—a field study and interpretation of the turbulent kinetic energy budget for high wave ages. J Atmos Sci 66:2764–2779

Högström U, Rutgersson A, Sahlée E, Smedman A, Hristov TS, Drennan WM, Kahma KK (2013) Air–Sea interaction features in the Baltic Sea and at a Pacific trade-wind site: an inter-comparison study. Bound Layer Meteorol 147:139–163. doi:10.1007/s10546-012-9776-8

Holthuijsen LH (2007) Waves in Oceanic and Coastal Waters. Cambridge University Press, 387 pp
Hoskins BJ, Hodges KI (2002) New perspectives on the Northern Hemisphere winter storm tracks. J Atmos Sci 59:1041–1061
Hurrell JW (1995) Decadal trends in the North Atlantic Oscillation and relationships to regional temperature and precipitation. Science 269: 676–679
Hurrell JW (1996) Influence of variations in extratropical wintertime teleconnections on Northern Hemisphere temperature. Geophys Res Lett 23:665–668
Hurrell JW, Van Loon H (1997) Decadal variations in climate associated with the North Atlantic Oscillation. Climate Change 36:301–236
IPCC (2013) In: Stocker TF, Qin D, Plattner G-K, Tignor M, Allen SK, Boschung J, Nauels A, Xia Y, Bex V, Midgley PM (eds) The physical science basis. Contribution of working group I to the fifth assessment report of the Intergovernmental Panel on Climate Change. Cambridge University Press, Cambridge
Janssen PAEM (2012) Ocean Wave Effects on the Daily Cycle in SST. J Geophys Res 117: C00J32, doi:10.1029/2012JC007943
Janssen PAEM, Doyle JD, Bidlot J-R, Hansen B, Isaksen L, Viterbo P (2002) Impact and feedback of ocean waves on the atmosphere. In: Perrie W (ed) Advances in Fluid Mechanics - Atmos.-Ocean Interact. WIT press, Ashurst, pp 155–197
Janssen PAEM, Breivik O, Mogensen K, Vitart F, Balmaseda M, Bidlot J, Keeley S, Leutbecher M, Magnusson L, Molteni F (2013) Air-sea interaction and surface waves, European Centre for Medium-Range Weather Forecasts. Tech Memo 712:36
Jeffreys H (1924) On the formation of waves by wind. Proc R Soc A107: 189–206
Jeffreys H (1925) On the formation of waves by wind. II. Proc R Soc A110:341–347
Jiang H, Chen G (2013) A global view on the swell and wind sea climate by the Jason-1 mission: a revisit. J Atmos Ocean Technol 30:1833–1841
Kinsman B (1965) Wind waves. Prentice-Hall, Englewood Cliffs, p 676
Komen GJ, Cavaleri L, Doneland M, Hasselmann K, Hasselmann S, Janssen P.A.E.M. Eds (1994) Dynamics and Modelling of Ocean Waves. Cambridge University Press, Cambridge, p 532
Lionello P, Galati MB (2008) Links of the significant wave height distribution in the Mediterranean sea with the North Hemisphere teleconnection patterns. Adv Geosci 17:13–18
Lionello P, Malguzzi P, Buzzi A (1998) Coupling between the atmospheric circulation and the ocean wave field: an idealized case. J Phys Ocean 28:161–177
Lucas C, Boukhanovsky A, Guedes SC (2011) Modelling the climatic variability of directional wave spectra. Ocean Eng 38(11–12):1283–1290
Luo D, Diao Y, Feldstein SB (2011) The variability of the atlantic storm track and the North Atlantic Oscillation: a link between intraseasonal and interannual variability. J Atmos Sci 68:577–601
Munk WH (1944) Proposed uniform procedure for observing waves and interpreting instrument records. Scripps Institution of Oceanography, Wave Project Rep. 26, 22 pp
Nilsson EO, Rutgersson A, Smedman A-S, Sullivan PP (2012) Convective boundary-layer structure in the presence of wind-following swell. Q J R Meteorol Soc 138:1476–1489. doi:10.1002/qj.1898
Pierson WJ, Moskowitz L (1964) A proposed spectral form for fully developed wind seas based on the similarity theory of S. A. Kitaigorodskii. J Geophys Res 69:5181–5190
Pilar P, Guedes SC, Carretero JC (2008) 44-year wave hindcast for the North East Atlantic European coast. Coast Eng 55:861–871
Ranjha R, Svensson G, Tjernström M, Semedo A (2013) Global distribution and seasonal variability of coastal low-level jets derived from ERA-Interim reanalysis. Tellus A 65:20412. doi:10.3402/tellusa.v65i0.20412
Reistad M, Breivik Ø, Haakenstad H, Aarnes OJ, Furevik BR (2011) A high-resolution hindcast of wind and waves for the North Sea, the Norwegian Sea and the Barents Sea. J Geophys Res 116, C05019
Rutgerson A, Saetra Ø, Semedo A, Carlson B, Kumar R (2010) Impact of surface waves in a Regional Climate Model. Meteorol Z 19(3):247–257
Rutgersson A, Nilsson EO, Kumar R (2012) Introducing surface waves in a coupled wave-atmosphere regional climate model: Impact on atmospheric mixing length. J Geophys Res 117: C00J15. doi:10.1029/2012JC007940
Semedo A (2010) Atmosphere–ocean Interactions in Swell Dominated Wave Fields. Ph.D. thesis. Uppsala University, Sweden. Available at http://www.diva-portal.org/smash/get/diva2:350126/FULLTEXT01.pdf
Semedo A, Sætra Ø, Rutgersson A, Kahma K, Pettersson H (2009) Wave-induced wind in the marine boundary layer. J Atmos Sci 66:2256–2271
Semedo A, Sušelj K, Rutgersson A, Sterl A (2011a) A global view on the wind sea and swell climate and variability from ERA-40. J Clim 24(5):1461–1479
Semedo A, Rutgersson A, Sterl A, Sušelj K (2011b) The global wave age climate. In: Soares G et al (eds) Marine engineering and technology. Taylor and Francis Group, London, pp 539–543
Semedo et al (2013) Projection of global wave climate change towards the end of the 21st century. J Clim 26:8269–8288
Smedman A, Hoögström U, Bergström H, Rutgersson A, Kahma KK, Petterson H (1999) A case study of air–sea interaction during swell conditions. J Geophys Res 104:25 833–25 852
Smedman A-S, Högström U, Sahleé E, Drennan WM, Kahama KK, Pettersson H, Zhang F (2009) Observational study of marine atmospheric boundary layer characteristics during swell. J Atmos Sci 66: 2747–2763
Smith SD, Anderson RJ, Oost WA, Coauthors (1992) Sea surface wind stress and drag coefficients: the HEXOS results. Bound-Layer Meteor 60:109–142
Snodgrass FE, Groves GW, Hasselmann KF, Miller GR, Munk WH, Powers WM (1966) Propagation of swell across the Pacific. Philos Trans R Soc Lond A259:431–497
Soares PMM, Cardoso R, Semedo A, Chinita MJ, Ranjha R (2014) The Iberian Peninsula Coastal Low Level Jet. Tellus A 66:22377. doi:10.3402/tellusa.v66.22377
Sterl A (2004) On the (in-)homogeneity of reanalysis products. J Clim 17: 3866–3873
Sterl A, Caires S (2005) Climatology, variability and extrema of ocean waves: the web-based KNMI/ERA-40 wave atlas. Int J Climatol 25: 963–977
Stopa J, Cheung KF (2014) Intercomparison of wind and wave data from the ECMWF Reanalysis Interim and the NCEP Climate Forecast System Reanalysis. Oc Model 75:65–83
Sullivan PP, Edson JB, Hristov T, McWilliams JC (2008) Large eddy simulations and observations of atmospheric marine boundary layers above nonequilibrium surface waves. J Atmos Sci 65:1225–1245
Tuomi L, Kahma KK, Pettersson H (2011) Wave hindcast statistics in the seasonally ice covered baltic sea. Boreal Environ Res 16:451–472
Undén P, Coauthors (2002) HIRLAM-5 scientific documentation. HIRLAM-5 Project, SMHI Tech. Rep. S-601 76, 144 pp
Uppala SM (1997) Observing system performance in ERA. ECMWF Re-Analysis Final Rep. Series 3, 261 pp
Uppala SM, Coauthors (2005) The ERA-40 re-analysis. Q J Roy Meteor Soc 131:2961–3012
Vikebø F, Furevik T, Furnes G, Kvamstø NG, Reistad M (2003) Wave height variations in the North Sea and on the Norwegian Continental Shelf, 1881–1999. Cont Shelf Res - CONT SHELF RES 23(3):251–263. doi:10.1016/S0278-4343(02)00210-8
Visbeck MH, Hurrel JW, Polvani L, Cullen HM (2001) The North Atlantic Oscillation: past, present, and future. Proc

Natl Acad Sci USA 98:12876–12877. doi:10.1073/pnas.231391598

WAMDI Group (1988) The WAM model—a third generation ocean wave prediction model. J Phys Oceanogr 18:1775–1810

Wang XL, Swail VR (2001) Changes of extreme wave heights in Northern Hemisphere oceans and related atmospheric circulation regimes. J Clim 14:2204–2221

WASA Group (1998) Changing waves and storms in the northeast Atlantic? Bull Am Meteorol Soc 79:741–760

Weisse R, Günther H (2007) Wave climate and long-term changes for the Southern North Sea obtained from a high-resolution hindcast 1958–2002. Ocean Dyn 57:161–172

Weisse R, Von Storch H, Feser F (2005) Northeast Atlantic and North Sea storminess as simulated by a regional climate model during 1958–2001 and comparison with observations. J Clim 18:465–479

Woolf DK, Challenor PG, Cotton PD (2002) Variability and predictability of the North Atlantic wave climate. J Geophys Res C (Oceans) 107(C10):3145–3149